Modeling and Control of a Bio-Inspired Underwater Vessel with Undulating-Fin Propulsion

Conference Paper · October 2018

DOI: 10.1109/OCEANS.2018.8604543

2 authors:

Mohammad Irfan Uddin
Florida Atlantic University
2 PUBLICATIONS **0** CITATIONS
SEE PROFILE

Oscar M Curet
Florida Atlantic University
37 PUBLICATIONS **399** CITATIONS
SEE PROFILE

Modeling and Control of a Bio-Inspired Underwater Vessel with Undulating-Fin Propulsion

Mohammad I. Uddin
Dept. of Ocean and Mechanical Engineering
Florida Atlantic University
Boca Raton, FL, USA
Email: muddin2017@fau.edu

Oscar M. Curet
Dept. of Ocean and Mechanical Engineering
Florida Atlantic University
Boca Raton, FL, USA
Email: ocuret@fau.edu

Abstract

Undulating-fin propulsion, where an elongated membrane is used to generate thrust, can enhance the mobility and station keeping capabilities of underwater vessels. Fish using this type of propulsion are able to maneuver in multiple directions including forward, backward, rapid reverse, upward, forward-lateral and station-keeping. Despite this potential, the use of undulating fin propulsion to control the six-degree of freedom of an underwater vessel has remained elusive, in part due to the lack of platform that allows studying the dynamics in free-swimming conditions. In this work, we present a self-contained physical model equipped with a bio-inspired fin-based propulsion. The propulsive mechanism is a single undulating fin running along the length of the robot, which controls both forward motion and directional maneuvers. We present a hydrodynamic characterization of the vessel in addition to a modeling framework to estimate forces, torques and motion control. As first step, we focus on the control for surge, sway and yaw.

Keywords: Underwater robotics, Bio-inspired propulsion, Undulating fin

Introduction

Although the control of unmanned underwater vehicles (UUV's) has received considerable attention in the last decades [1-12], the navigation in tight spaces and near-objects in complex underwater environments (e.g. waves, cross-currents, turbulence) remain a challenge. Currently, most UUVs utilize one or multiple propeller to generate thrust. Single thrusters are generally used with hydro-planes or robotic wrist for turning, but in these configurations, the vehicle needs to move horizontally in order to move in other directions. Multiple thrusters can also be used for turning or motion control, however drag and streamline of the vehicle is highly impacted, thus diminishing its efficiency. A bio-inspired underwater vessel with undulating fin propulsion can provide multiple advantages for the navigation in such complex environments.

In ribbon-fin-based locomotion, thrust is generated by traveling waves along an elongated fin while the body is kept mainly straight Figure 1. The motivation of this study is to determine the interconnection between fin kinematics and turning performances of ribbon-fin-based propulsion to obtain a motion control model. As a first step toward that goal, we focus in the motion in a horizontal plane.

The wide range of force direction is one of the great advantages of undulating fin propulsion. It has been observed, that one or multiple traveling waves along the fin can be used to generate forward or backward motion, as well as impressive maneuvers [13][14]. In addition, counter-colliding travelling waves can enable precise station-keeping or even vertical motion [15][16]. However, an understanding of how to efficiently manipulate the fin kinematics in a robotic underwater vessel to generate specific maneuvers is not well understood.

One of the challenges of controlling the motion of a vessel using undulating fin propulsion is the extensive parameter space of the propulsive surface. For a single vessel with fin-based propulsion the key parameters (Figure 2A) includes: 1) the actuation parameters for each ray: frequency, amplitude of oscillation along the fin, and phase difference from each ray to form a specific wavelength [16-18]; 2) geometry considerations: fin morphology [19], length scales, and spacing between rays; 3) elastic properties of the rays and the membranes [19], 4) actuation level: passive versus active control of the rays [20]. Even though there has been considerable progress made toward understanding ribbon-fin-based propulsion, details regarding motion control have not been investigated in detail. Previous studies on undulating fin propulsion using robotic devices mainly focused on the thrust generation [16] [23], fin kinematics [13][24], efficiency [19-22][34], hydrodynamics [17][26][27] and swimming efficiency for straight/backward swimming and hovering [21-22].

As crucial step toward the motion control of a freely-swimming vessel propelled by an undulating fin, this work focuses on a simple thrust vectoring (Figure 2B) of the force generated to control forward swimming and yaw turning. In this thrust vector approach, the undulating fin is divided in two sections along the length of the fin where the trailing segment is deviated from the longitudinal axis to generate a force component in both surge and sway direction and therefore providing a yaw moment to turn the vessel. Using this simple approach, we focus to understand, what are the turning performance of the vessel, as well as the angle and length of the trailing segment that provide better performance for turning. In particular, we want to explore if there is an optimal point for the divide the fin (or breaking point, x_{br}). In this work, we provide an initial framework to study this problem with simulations, laboratory experiments and preliminary field experiments (Figure 2C-D).

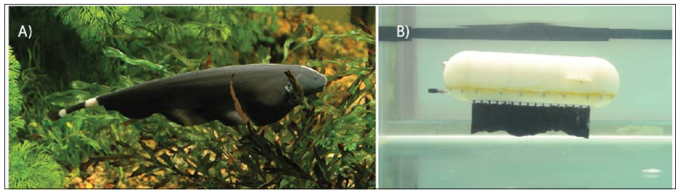

Figure 1: A) The black ghost knifefish (Apteronotus albifrons) from South America. (Photo courtesy of Per Erik Sviland). B) The robotic underwater vessel-- the Knifebot -- with undulating fin propulsion.

Materials and Methods

The Knifebot

We have built a self-contained bio-inspired underwater vessel with single undulating fin running along the length of the robot, which control both forward motion and directional maneuvers [21][22]. This novel biomimetic vessel features a compact slender 3D-printed hull with 16 DC motors, 2 Li-Ion batteries and 5 electronic boards encapsulated inside the vessel. The hull of the vessel is 462 mm long (L_{hull}), 77 mm wide (W_{hull}) and 125 mm high (H_{hull}). The undulating fin is composed of 16 rays that are interconnected with a flexible and elastic membrane made of a Lycra fabric, that is 300 mm long (L_{fin}) and 70 mm high (H_{fin}). Each ray is actuated by a separate DC motor. An inertial measurement unit (IMU) is used to measure linear accelerations, orientation angles and rotational velocities. In addition, the vessel has sensors for leakage detection, power consumption and pressure and temperature monitoring. We successfully replicated different maneuvers including: forward swimming, diving, reversed motion and station keeping, as well to demonstrate vertical swimming using counter-propagating waves ([21], [22]).

Governing Equations

One of the motivations of this work is to develop a mathematical simulation model for the vessel. To achieve this goal, we considered 3 2nd order differential equations. These 3 equations are function of surge, sway and yaw motions respectively.

$$M(1 + A_{surge})\ddot{x} = F_{T,surge} - F_{D,surge} \quad (1)$$
$$M(1 + A_{sway})\ddot{y} = F_{T,sway} - F_{D,sway} \quad (2)$$
$$I(1 + A_{yaw})\ddot{\omega} = M_{T,yaw} - M_{D,yaw} \quad (3)$$

Here,
M= mass of vessel
I = mass moment of inertia in yaw
A_{surge} = added mass coefficient in surge
A_{sway} = added mass coefficient in sway
A_{surge}= added mass moment of inertia in yaw
$F_{T,surge}$ = net force generated by the fin in surge
$F_{D,surge}$ = vessel drag in surge
$F_{T,sway}$ = net force generated by the fin in sway
$F_{D,sway}$ = vessel drag in sway
$M_{T,yaw}$ = net yaw moment generated by the fin
$M_{D,yaw}$ = vessel drag moment in yaw

From equation (1), (2) and (3)**,** we can observe that surge motion equation is only dependent on surge velocity and acceleration, whereas the other two equations (sway and yaw) have interdependent parameters. More detailed explanation of the force terms will be provided in the later part of this paper.

Experimental Setup

In addition to theoretical prediction, we conducted towing experiment in a wave tank located at the hydrodynamic lab facility in SeaTech campus at Florida Atlantic University (FAU). The wave tank is 4 feet wide, 4 feet wide and 60 feet long. This tank is equipped with a carrier for towing experiments (Figure 2C). The motor driver can be accessed and control by computer, using a dedicated software for the motor driver (Anaheim Automation SMC60win – Version2.01). This motor driver is capable of generating precise velocity and acceleration of the carriage, where the vessel is mounted through a load cell (see Figure 2C). We used Futek load cell (LSB 200), with maximum 1lb load capacity. After load cell was attached to the mounting, the sensing side of the load cell was then attached to the vessel, through the other mounting. All connection from the vessel to the carrier were firmly secured to avoid any relative motion.

For data acquisition, we set a laptop in the carrier, which was accessed by remote desktop connection. The load cell was attached to an amplifier (manufacturer: Futek, model CSG110). The amplifier is then connected to the data acquisition board (National Instrument 194710D-04L), which was then connected to the laptop installed in the carriage. We acquired data at a sampling frequency of 1000 Hz.

We conducted two different sets of experiments. The first set was to characterize the drag of the vessel. During this experiment, the carrier was towed at 14 different speeds, roughly from 50 cm/s (0.167 L_{fin}/s) upto 700 mm/s (2.33 L_{fin}/s),

without actuating the fin and with the fin straight ($\theta = 0^o$). The Reynolds number was defined as, $Re = U_{sw}L_{hull}/\upsilon$, where U_{sw} is the translational speed of the vessel (same as the carrier speed), and υ is the kinematic viscosity of the water. The Reynolds number ranged between $2x10^4$ and $3.5x10^5$. The drag measurements were obtained after reaching the steady state velocity of the carrier. The drag measurement range from 1 to 3 minutes depending on the speed of the carrier. For the second set of experiment, we actuated the fin with no carrier motion ($U_{sw} = 0$). The fin was actuated for 6 different frequencies from 0.5-3 Hz (at 0.5 Hz interval) and keeping the wavelength constant at 15 cm ($\lambda = L_{fin}/2$). Each case of all the thrust experiments were ran three times, each run taking more than 60 seconds.

Simulation

We performed a series of simulations for motion in surge, sway and yaw. To perform yaw turning the fin was divided in two segments -- a leading and a trailing section (Figure 2B). x_{br} is the aft part length of the fin and angle of α is the deviation of this segment with respect to the longitudinal axis. The forward length of the fin is given by L_{fin} - x_{br}. The mean deflection angle of the forward segment was always aligned with the center line. When actuated, the fore part generates a mean thrust force purely acting in the surge direction, as given below

$$F_{x1}(x_{br}) = \frac{1}{2}\, C_t\, \rho\, A_{e1} \left(V_{wave} - U_x\right)^2 \quad (4)$$

$F_{x1}(x_{br})$ = Surge force generated by forward centerlined portion, with length (L_{fin} - x_{br})
C_t = Trust coefficient
ρ = Density of water
A_{e1} = Swept area of the fore portion of the fin = $2\, H_{fin}\, \sin\theta\, (L_{fin} - x_{br})$
V_{wave} = Wave velocity of the fin = $f\lambda$
f= Frequency of travelling wave
λ=Wave length of the fin wave
U_x= Surge component of swimming velocity of the vessel
θ = Maximum angular amplitude of the fin from z-axis
L_{fin} = Total length of fin

The force generated by rear portion (x_{br}) can be calculate as follows

$$F_2(x_{br}, \alpha) = \frac{1}{2}\, C_t\, \rho \left(2\, H_{fin}\, sin\theta\, x_{br}\right)\left(V_{wave} - U_x \cos\alpha - U_y \sin\alpha\right)^2 \quad (5)$$

where
$F_2(x_{br}, \alpha)$ = force generated by the rear portion, x_{br}, along the fin
H_{fin} = height of fin= 70 mm
α = angle of the rear portion of the fin with respect to the center line
U_y = sway component of swimming velocity of the vessel

The force generated by the rear portion can be subdivided into two components, i.e. surge and sway. In addition, the sway force (and surge) results in yaw moment, which causes the vessel to turn. For this calculations it is assumed that the F_2 is acting in the middle of rear section. The components in surge, sway as well as the yaw moment of F_2 are given by equation (6), (7) and (8).

$$F_{x2}(x_{br}, \alpha) = F_2 \cos\alpha \quad (6)$$
$$F_{sway}(x_{br}, \alpha) = F_2 \sin\alpha \quad (7)$$
$$M_{yaw}(x_{br}, \alpha) = F_2 \times L_{yaw} \quad (8)$$

Here,
$F_{x2}(x_{br}, \alpha)$ = surge component of force F_2
L_{yaw} = moment arm length of F_2 with respect to the center of gravity (at midship).

F_{sway} and M_{yaw} are the total sway and yaw moment of the system, referenced in equation 2 and 3 respectively. Now, the total surge force, F_{surge}, can be expresses as given in equation (9).

$$F_{surge} = F_{x1} + F_{x2} \quad (9)$$

The equations for drag forces considered in this paper are based on the work done by Deng. et al. (2004) [28]. The drag force and moments are proportional to the square of linear and angular velocity of the vessel respectively. These forces can be expressed as equations (10), (11) and (12).

$$F_{D,surge} = X_{Duu}|U_x|U_x \quad (10)$$
$$F_{D,sway} = Y_{Dvv}|U_y|U_y \quad (11)$$
$$M_{D,yaw} = N_{Drr}|\omega_z|\omega_z \quad (12)$$

Where,

$$X_{Duu} = \frac{1}{2}\, \rho\, C_{D,\, surge} A_{p,\, x}$$

$$Y_{Dvv} = Y_{Dvv}^{hull} + Y_{Dvv}^{fin}$$

$$Y_{Dvv}^{hull} = -\frac{1}{2}\, \rho\, C_{dc} \int_{-\frac{L_{hull}}{2}}^{\frac{L_{hull}}{2}} 2\, H_{hull}\, dx$$

$$Y_{Dvv}^{fin} = -\frac{1}{2}\, \rho\, A_{fin}\, C_{D,\, fin}$$

$$N_{Drr} = -\frac{1}{2}\, \rho\, C_{dc} \int_{-\frac{L_{hull}}{2}}^{\frac{L_{hull}}{2}} 2x^2|x|\, H_{hull}\, dx$$

$A_{p,\ x}$ = frontal area of the vessel = $\pi \times \frac{(H_{hull} \times W_{hull})}{4}$
C_t = thrust coefficient
$C_{D,\, surge}$= drag coefficient for hull
$C_{D,\, fin}$= drag coefficient of fin in sway = 1
ρ= density of water = 1000 kg/m^3
L_{hull}= length of hull = 462mm
H_{hull} = height of the hull = 125 mm
W_{Hull} = width of hull = 77 mm

For all the simulations the coefficient of drag was taken as 0.86, as a cylinder [28] and the coefficient of thrust was taken as 0.5 [19].

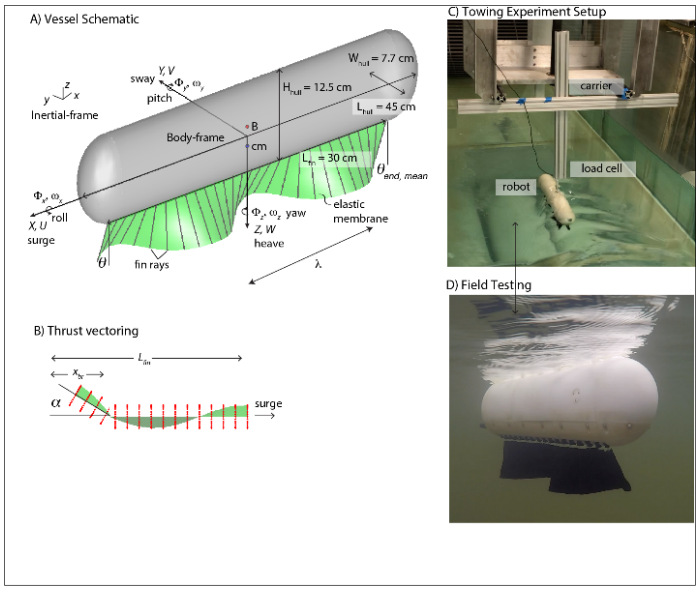

Figure 2: A) Schematic Diagram of the Knifebot, defining all 6 degrees of freedom. B) Schematic diagram for fin configuration for yaw turning. C) Experimental setup for drag force measurement in towing tank at Hydrodynamic Lab at Dania Beach campus of FAU. D) Picture of Knifebot, captured during field run at intercostal at Dania Beach, Florida

Using equations 1, 4 and 10, we created simulation model in Matlab for straight trajectory of the vessel (considering $x_{br} = 0$). For this case, mean position of the fin was vertically aligned with the center line of the body, causing no forces in sway and yaw.

In addition we model a straight swimming followed by a yaw turning due to the deflection of the mid-center axis of the rear portion of the fin. For this case, equations 1-10 were used. The time step set for both simulations was 0.01s. After each time step, the position of the vessel was updated.

Results and Discussion

Drag characterization

The towing experiments were performed to characterize the drag of the vessel. Figure 3A shows the drag measurement with respect to time when the vessel is towed at a speed of 199.49 mm/s. For each swimming speed, the drag force was calculated from the mean of three different measurements, where each measurement comes from a separate time series data. Figure 3B shows the mean drag force measured as a function of towing speed. Here, a gradual increase of the drag with the swimming speed is observed. In addition, the drag coefficients are plotted against Reynolds number (*Re*) (Figure 3C). The drag coefficient varies roughly between 0.8 and 0.5. It should be mentioned that both the body and fin of the vessel has contribution to this drag coefficient. For Reynolds number between 2.5×10^4 and 3×10^5, a drop in the drag coefficient is observed. This drop in drag coefficient is most likely due to the development of turbulent wake behind the vessel.

Thrust characterization

Holding the vessel in a fixed position, we measured the thrust forces produced by the fin, for different combination of fin frequency and a constant wavelength. *Figure 4* depicts force generated by the fin as a function of time (Figure 4A), the mean surge force as a function of wave speed (Figure 4B) and the mean thrust coefficient (Figure 4C). presented. Similar to previous studies [16,19], the mean thrust generated by the fin increases exponentially with wave speed until a certain point that it diminish or the rate of increment decreases. This can be clearly observed in the thrust coefficient that is fairly constant at around 0.4 – 0.45 for wave speed less than 1 L_{fin}/s but decreases for higher wave speeds.

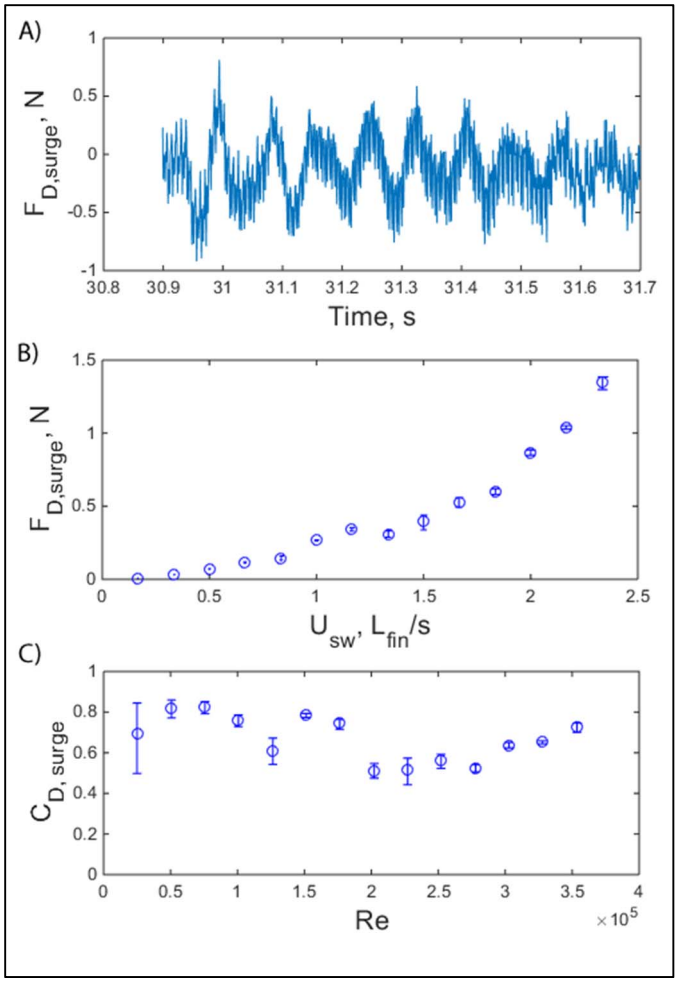

Figure 3: A) Time series of Drag force in forward motion, at 1000 Hz sampling freq. B) Mean drag in surge direction as a function of swimming speed. C) Drag coefficient as function of Reynolds number.

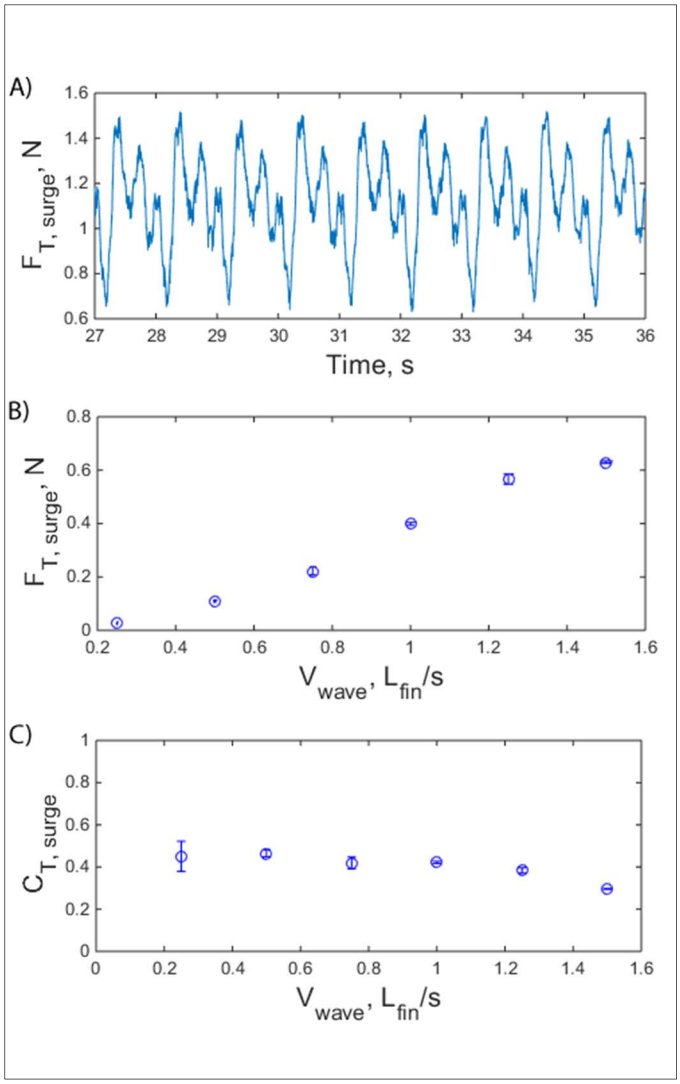

Figure 4: A) Time series of Thrust force in forward motion, at 1000 Hz sampling freq. The fin was actuated with 15cm wavelength (0.5 L_{fin}/s), and frequency of 1 Hz. B) Plot for Thrust force generated at surge direction. In this case, the fin was actuated for 6 different cases, with 15cm wavelength, and frequency between 0.5-3 Hz. This result in V_{wave} between 0.075-0.45 m/s. C) Plot for non-dimensional Thrust coefficient as a function of wave speed, corresponding to the Thrust force plotted at figure B

Figure 5 compares simulated and experimental steady state surge velocities reached by the vessel as a function of wave speed. The simulated values are show in blue dots while experimental values are shown color coded from light yellow to dark red. The filled and open circles are experimental data for one or two undulations along the fin. At lower velocities (close to 1 L_{fin}/s), the simulated steady state velocities are in good agreement with the experimental velocities.

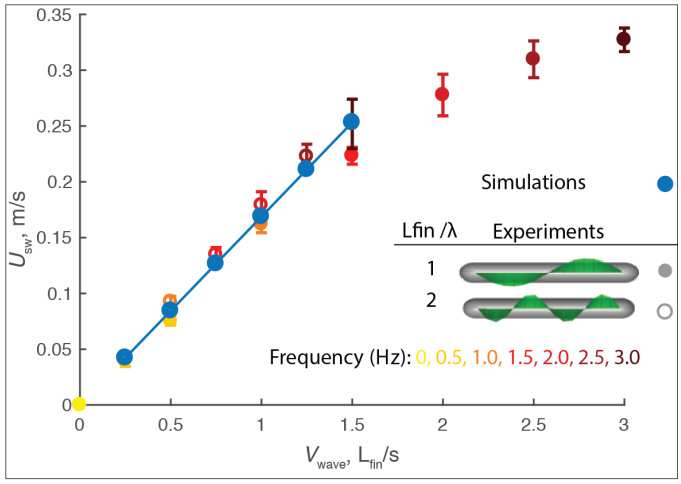

Figure 5: Comparison between simulated vs experimental swimming speed of the vessel. The solid blue dots simulated results from simulation, whereas other filled and non-filled circles shows experimental results for wavelengths of 30cm and 15cm respectively [21]. *For lower swimming speeds (<1.25 L_{fin}/s), simulation results reasonably agree to experimental results.*

Figure 6 shows simulated yaw moment (M_{yaw}), plotted as a function of x_{br} and $\theta_{end,\ mean}$. $\theta_{end,\ mean}$ is the mean deflection velocity of the last ray in the fin (see Fig. 2A) M_{yaw} is proportional the $\theta_{end,\ mean}$, but does not show monotonous dependency with x_{br}/L_{fin} . The maximum value of M_{yaw} occurs between 13-20% value of x_{br}/L_{fin} , which suggests that for yaw moment, an optimal subdivision point of fin can exist at this interval

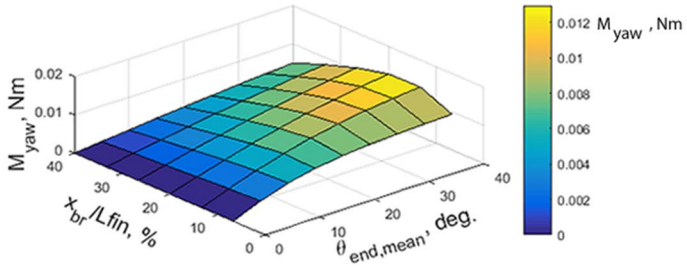

Figure 6: Yaw moment from simulation as a function of x_{br} and mean angle at end of fin ($\theta_{end,\ mean}$)

Figure 7 shows variation of linear and angular velocities, heading angle, forces and torque during a straight trajectory followed by yaw turning. Initially, the vessel accelerates from a static position, accelerating in forward direction. After 10 sec (the surge velocity reaches the steady state value by this time), the aft part of the fin is deflected, which causes yaw turning of the vessel. At this point, the sway force ($F_{T,\ Sway}$) and yaw moment ($M_{T,\ yaw}$) reaches maximum. As time progresses, the sway velocity increases, resulting in an increase in sway drag forces ($F_{D,\ sway}$) and decrease in sway thrust force ($F_{T,\ sway}$). Gradually, these two forces becomes equal, and the sway velocity reaches its steady state condition. Similar phenomenon happens for yaw motion as well. As a result, after finite time,

the system reaches steady surge, sway and yaw velocities that enables the system to demonstrate steady turning characteristics (Figure 8) reaching a circular yaw turn.

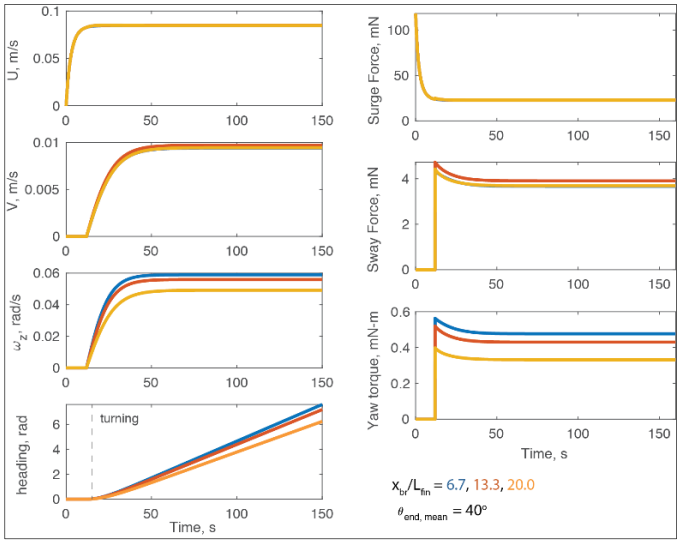

Figure 7: Simulated vessel velocities and fin forces/torques during a first straight trajectory followed by a turning (after 10 seconds). Left columns show the velocity in surge, U, sway, V, rotational velocity, omega and heading. Right column shows surge force, sway force and yaw torque generated by the fin.

Figure 8 shows the simulated turning path of the vessel, for the cases considered in Figure 7. Figure 8A shows three different trajectories, for varying x_{br}/L_{fin}, keeping $\theta_{end,mean}$ constant. The turning circle becomes smaller for lower value of x_{br}. Again, Figure 8B shows 2 different plots, with different values of $\theta_{end,mean}$ (40º and 45º), and constant value of x_{br}/L_{fin} (6.7%). The turning radius decreases with increase of $\theta_{end,mean}$.

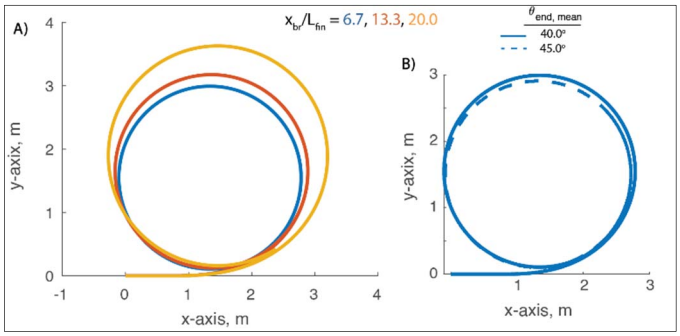

Figure 8: Simulated path of the vessel for a straight motion followed by a turning due to a deflection of the fin. Left panel show the path for three different breaking points with same deflection of the extreme end of the fin, $\theta_{end,\ mean}$ = 40º. Right panel shows the vessel path for two fin deflection with same braking point x_{br}/L_{fin}= 6.7

Conclusions

In this paper, we present a modeling and potential turning approach of a bio-inspired underwater vessel with a single undulating fin. In particular, we investigated a thrust vectoring approach to control both forward and turning maneuvers. In addition, we measured the drago f the ve in surge direction with towing experiments. In addition, we measured the thrust generation of the undulating fin when the vessel was stationary. A simulation framework was presented to analyse the motion of the vessel for different fin kinematics including forward motion and yaw turning. Yaw moment simulation results suggest that an optimal breaking point of the fin can exist for efficient turning of the vessel. The straight trajectory simulations, obtained by solving surge force equations, are reasonable when compared with results from earlier experiments done on the same device by Liu and Curet [21]. In addition, based on the work done by earlier researchers [28], we proposed a simulation model for yaw turning for the present vessel. The validation of these results are subjected to future experiments. In addition, coupled drag and thrust force experiments should validate our present experimental results, as well as the straight trajectory simulations.

ACKNOWLEDGMENT

This material is based upon work supported by the National Science Foundation under Grant No. 1751548 to O.M.C

I. REFERENCES

[1] R. Cristi, F. A. Papoulias and A. J. Healey, "Adaptive sliding mode control of autonomous underwater vehicles in the dive plane," *IEEE J Ocean Eng.,* pp. 152-160, 1990.

[2] O. Fjellstad and T. I. Fossen, "Quaternion feedback regulation of underwater vehicles," *3rd IEEE Conference on Control Application,* 1994.

[3] T. I. Fossen, Guidance and control of ocean vehicles, John Wiley & Sons Inc, 1994.

[4] P. Frihauf, S. Liu and M. Krstic, "A single forward-velocity control signal for stochastic source seeking with multiple nonholonomic vehicles," *Journal of Dynamic Systems, Measurement, and Control,* vol. 136, no. 5, p. 051024, 2014.

[5] A. J. Healey and D. Lienard, "Multivariable sliding mode control for autonomous diving and steering of unmanned underwater vehicles," *IEEE J Ocean Eng.,* vol. 18, no. 3, pp. 327-39, 1993.

[6] D. L. Juul, M. McDermott, E. L. Nelson, D. M. Barnett and G. N. Williams, "Submersible control using the linear quadratic gaussian with loop transfer recovery method,"

Proceedings of IEEE Symposium on Autonomous Underwater Vehicle Technology (AUV'94), 1994.

[7] N. E. Leonard, "Periodic forcing, dynamics and control of underactuated spacecraft and underwater vehicles," in *Proceedings of the 34th IEEE Conference on Decision and Control*, 1995.

[8] N. E. Leonard and J. E. Marsden, "Stability and drift of underwater vehicle dynamics: mechanical systems with rigid motion symmetry," *Physica D.,* vol. 105, no. 1-3, pp. 130-62, 1997.

[9] P. Tsiotras, "Stabilization and optimality results for the attitude control problem," *Journal of Guidance, Control, and Dynamics,* vol. 19, no. 4, pp. 772-9, 1996.

[10] S. B. Williams, P. Newman, G. Dissanayake, J. Rosenblatt and H. Durrant-Whyte. "A decoupled, distributed AUV control architecture," *International Symposium on Robotics*, 2000

[11] D. M. Boskovic and M. Krstic, "Global attitude/position regulation for underwater vehicles," *Int J Syst Sci.,* vol. 30, no. 9, pp. 939-46, 1999.

[12] N. E. Leonard and J. E. Marsden, "Stability and drift of underwater vehicle dynamics: mechanical systems with rigid motion symmetry," *Physica D.,* vol. 105, no. 1-3, pp. 130-62, 1997.

[13] R. Ruiz-Torres, O. M. Curet, G. V. Lauder and M. A. MacIver, "Kinematics of the ribbon fin in hovering and swimming of the electric ghost knifefish," *J Exp Biol.,* vol. 216, no. 5, pp. 823-34, 2013.

[14] M. A. Maciver, N. M. Sharabash and M. E. Nelson, "Prey-capture behavior in gymnotid electric fish: motion analysis and effects of water conductivity," *J Exp Biol.,* vol. 204, no. 3, pp. 543-57, 2001.

[15] S. Sefati, I. Neveln, M. A. MacIver, E. S. Fortune and N. J. Cowan, "Counter-propagating waves enhance maneuverability and stability: a bio-inspired strategy for robotic ribbon-fin propulsion," in *4th IEEE RAS & EMBS International Conference on Biomedical Robotics and Biomechatronics (BioRob)*, 2012.

[16] O. M. Curet, N. A. Patankar, G. V. Lauder and M. A. MacIver, "Mechanical properties of a bio-inspired robotic knifefish with an undulatory propulsor," *Bioinspiration & biomimetics,* vol. 6, no. 2, p. 026004, 2011.

[17] I. D. Neveln, Y. Bai, J. B. Snyder, J. R. Solberg, O. M. Curet and K. M. Lynch, "Biomimetic and bio-inspired robotics in electric fish research," *Exp Biol,* vol. 217, no. 2, pp. 201-13, 2014.

[18] I. D. Neveln, R. Bale, A. P. S. Bhalla, O. M. Curet, N. A. Patankar and M. A. MacIver, "Undulating fins produce off-axis thrust and flow structures," *J Exp Biol.,* vol. 217, no. 2, pp. 201-13, 2014.

[19] H. Liu, B. Taylor and O. M. Curet, "Fin ray stiffness and fin morphology control ribbon-fin-based propulsion," *Soft Robotics,* vol. 4, no. 2, pp. 103-16, 2017.

[20] H. Liu and O. M. Curet, "Propulsive performance of an under-actuated robotic ribbon fin," *Bioinspiration & biomimetics,* 2017.

[21] H. Liu and O. M. Curet, "Swimming Performance of a Bio-Inspired Robotic Vessel with Undulating Fin Propulsion," *Bioinspiration & Biomimetics,* 2018.

[22] H. Liu, F. Gong and O. M. Curet, "Unleashing the Potential of Undulating Fin Propulsion Using a Biomimetic Robotic Vessel," *Marine Technology Society Journal,* vol. 51, no. 5, pp. 79-93, 2017.

[23] M. Epstein, J. E. Colgate and M. A. MacIver, "Generating Thrust with a Biologically-Inspired Robotic Ribbon Fin," *IEEE,* 2006.

[24] E. D. Youngerman, B. E. Flammang and G. V. Lauder, "Locomotion of free-swimming ghost knifefish: anal fin kinematics during four behaviors," *Zoology,* vol. 117, no. 5, pp. 337-48, 2014.

[25] R. Bale, I. D. Neveln, A. P. S. Bhalla, M. A. MacIver and N. A. Patankar, "Convergent evolution of mechanically optimal locomotion in aquatic invertebrates and vertebrates," *PLoS biology,* vol. 13, no. 4, p. e1002123, 2015.

[26] A. A. Shirgaonkar, O. M. Curet, N. A. Patankar and M. A. MacIver, "The hydrodynamics of ribbon-fin propulsion during impulsive motion," *J Exp Biol,* vol. 211, no. 21, pp. 3490-503, 2008.

[27] O. M. Curet, N. A. Patankar, G. V. Lauder and M. A. MacIver, "Aquatic manoeuvering with counter-propagating waves: a novel locomotive strategy," *Journal of The Royal Society Interface,* vol. 8, no. 60, pp. 1041-50, 2011.

[28] Z. Deng, M. C. Richmond and C. S. Simmons, Six-degree-of-freedom sensor fish design - governing equations and Motion Modelling, U.S. Department of Energy, 2004.